IN-93-A
26379
P-27

FINAL TECHNICAL REPORT

NASA GRANT NAGW-1247

"Cosmic Ray Positron Research and Silicon Track Detector Development"

1 Dec. 87 - 30 Nov. 90

Principal Investigators

12/1/87 - 9/11/88: W. Vernon Jones
9/11/88 - 11/30/90: John P. Wefel

Department of Physics and Astronomy
Louisiana State University
Baton Rouge, LA 70803-4001

Phone: 504-388-8696
Fax: 504-388-5855
E-Mail: WEFEL%PHEPDS.SPAN@LSUVAX.LSU.EDU

prepared for

National Aeronautics and Space Administration
Space Physics Division
Code SS
Washington, DC 20546

(NASA-CR-187706) COSMIC RAY POSITRON RESEARCH AND SILICON TRACK DETECTOR DEVELOPMENT Final Technical Report, 1 Dec. 1987 - 30 Nov. 1990 (Louisiana State Univ.) 27 p

N91-28059

Unclas
CSCL 03B G3/73 0026379

Cosmic Ray Positron Research and
Silicon Track Detector Development

NAGW-1247

I. Introduction

Grant NAGW-1247 was established at LSU in 1987 for the dual purposes of conducting research on:

a) position sensing detector systems, particularly those based upon silicon detectors, for use in future balloon and satellite experiments, and
b) positrons, electrons, proton, anti-protons and helium particles as measured by the NASA NMSU Balloon Borne Magnet Facility.

The research was to be conducted, mainly, off-campus at the Goddard Space Flight Center (GSFC) under the direction of W. V. Jones, LSU, and J. F. Ormes, GSFC, with Prof. Jones spending a considerable fraction of his time in the Washington, DC area. The effort was composed of a postdoctoral associate working on detector development at GSFC, a part-time postdoctoral associate and other staff working at LSU and a graduate student working on the data from the Balloon Borne Magnet Facility (BBMF) both at GSFC and at LSU.

Approximately half-way through the project, Prof. Jones retired from active status at LSU, becoming Professor Emeritus. With concurrence of NASA Headquarters, Prof. John P. Wefel replaced Prof. Jones as Principal Investigator to finish the work, particularly the analysis of the BBMF data with graduate student E. S. Seo. Also, due to hardware difficulties, the planned balloon flight schedule of the BBMF had to be altered. This shifted the focus of the data analysis away from e^+e^- in favor of $p,\bar{p}$ and p, He spectra. This also caused a delay in the project plan which necessitated a one-year's extension to the term of the grant.

Under grant NAGW-1247, we have made significant technical progress on a number of different position sensitive detector systems. Although no one system has been able to be completely developed for flight, the basic ground work has been established for the future development of such systems. In addition, a major advance has been made in the study of the rigidity spectra of the two most abundant cosmic ray species, Hydrogen and Helium, including analysis of re-acceleration effects in the Interstellar Medium.

The next section gives the Bibliography to work support wholly or in part by this grant. This is followed by a Summary of the Research Accomplished in the two principal areas covered by the project. The attachments include articles for which preprints or reprints are currently available.

II. Bibliography

A. Journal Publications/Book Chapters:

"Measurement of Cosmic Ray Proton and Helium Spectra During the 1987 Solar Minimum," E. S. Seo, J. F. Ormes, R. E. Streitmatter, S. J. Stochaj, W. V. Jones, S. A. Stephens and T. Bowen, Astrophysical Journal, Sept. 91 issue, in press (1991).

"The Composition of the Cosmic Rays – An Update," John P. Wefel, in Cosmic Rays, Supernovae and the Interstellar Medium, eds. M. M. Shapiro, R. Silberberg and J. P. Wefel, NATO ASI Series C, Vol. 337, (Dordrecht, The Netherlands; 1991; Kluwer Academic Publishers), p. 29.

"Central Collisions of 800 GeV Protons with Ag and Br Nuclei," Abduzhamilov, A., et al., (The Baton Rouge-Krakow-Moscow-Tashkent Collaboration), Physical Review, D39, 86, (1989).

B. Articles in Preparation/Submitted:

"Performance of a Balloon-Borne Magnet Spectrometer for Cosmic Ray Studies," R. L. Golden, C. Grimani, B. L. Kimbell, W. R. Webber, G. Basini, A. Morselli, M. Ricci, J. F. Ormes, E. S. Seo, S. J. Stochaj, R. E. Streitmatter, P. Spillantini, A. Codino, M. Menichelli, M. P. DePascale, F. Bongiorno, and P. Picozza, Nucl. Instr. Meth. (1991).

"Performance of focused Gas Cherenkov Detector Used for Cosmic Ray Studies," R. L. Golden, C. Grimani, B. L. Kimbell, W. R. Webber, G. Basini, A. Morselli, M. Ricci, J. F. Ormes, E. S. Seo, S. J. Stochaj, R. E. Streitmatter, P. Spillantini, A. Codino, M. Menichelli, M. P. DePascale, F. Bongiorno, and P. Picozza, Nucl. Instr. Meth. (1991).

C. Books:

Cosmic Gamma Rays, Neutrinos and Related Astrophysics, eds. M. M. Shapiro and J. P. Wefel, NATO ASI Series C, Vol. 270, (Dordrecht, The Netherlands; 1989; Kluwer Academic Publishers), 692 p.

D. Conference Proceedings:

"Cosmic Ray Proton Spectra at Low Rigidities," E. S. Seo, J. F. Ormes, R. E. Streitmatter, J. Lloyd-Evans and W. V. Jones, 21st Int. Cosmic Ray Conf. Papers (Adelaide), Vol. 3, p. 7, (1990).

"Experimental Limit on Low Energy Antiprotons in the Cosmic Radiation," R. E. Streitmatter, S. J. Stochaj, J. F. Ormes, R. L. Golden, S. A. Stephens, T. Bowen, A. Moats, J. Lloyd-Evans, L. Barbier, E. S. Seo, 21st Int. Cosmic Ray Conf. Papers (Adelaide), Vol. 3, p. 277, (1990).

"Positron Electron Magnet Spectrometer (POEMS) for the EOS Mission," P. Evenson, J. P. Wefel, S. Swordy, R. Streitmatter, M. Salamon, L. Barbier, T. G. Guzik, K. P. Magee-Sauer, J. W. Mitchell, J. F. Ormes, R. Ramaty and D. V. Reames, in Particle Astrophysics, eds. W. V. Jones, F. J. Kerr and J. F. Ormes, AIP Conference Proc. No. 203, (New York, 1990, American Institute of Physics), p. 58.

E. Dissertation:

"Measurement of Galactic Cosmic Ray Proton and Helium Spectra During the 1987 Solar Minimum" by Eun-Suk Seo, Louisiana State University (1991). Available from University Microfilms, Inc.

F. Abstracts:

"Micron Resolution Charged Particle Detectors," L. M. Barbier et al., Bull. Am. Phys. Soc., 33, (1988).

"Cosmic Ray Proton Spectra," E. S. Seo, J. F. Ormes, R. E. Streitmatter, S. J. Stochaj, R. L. Golden, T. Bowen, A. Moats and J. Lloyd-Evans, Bull. Am. Phys. Soc., 34, 1185 (1989).

"Cosmic Ray Protons and Helium Spectra, Splash Albedo from Solar Minimum, 1989," E. S. Seo, J. F. Ormes, R. E. Streitmatter, S. J. Stochaj, R. L. Golden, S. A. Stephens, T. Bowen, A. Moats and J. Lloyd-Evans, Bull. Am. Phys. Soc., 35, 1065 (1990).

"The Deuterium to He^4 Ratio Obtained with a Balloon Borne Superconducting Magnetic Spectrometer," S. J. Stochaj, E. S. Seo, R. E. Streitmatter, J. F. Ormes, R. L. Golden, S. A. Stephens, T. Bowen, A. Moats and J. Lloyd-Evans, Bull. Am. Phys. Soc., 35, 1065 (1990).

"Upper Limits on 100-1200 MeV Anti-Protons in the Cosmic Rays," R. E. Streitmatter, S. J. Stochaj, L. Barbier, J. F. Ormes, E. S. Seo, R. L. Golden, S. A. Stephens, T. Bowen, A. Moats and J. Lloyd-Evans, Bull. Am. Phys. Soc., 35, 1066 (1990).

III. Summary of the Research

Observations over the past several years have produced significant and unexpected results on the fluxes of cosmic ray particles arriving at earth, while parallel theoretical developments have provided a new framework for understanding the particles' origin, acceleration, and propagation through the interstellar medium. Concurrently, profound astrophysical questions have been raised by the lack of definitive observations of either proton decay or free magnetic monopoles, both of which are expected within the framework of the Grand Unified Theories. Recognizing the importance of these rapid changes, the Astrophysics Division in 1985 chartered a team of scientists to define the goals and requirements for a superconducting magnet facility (now called Astromag) to be operated for several years on the Space Station or as a free flyer. This step was followed by a restructuring of the Particle Astrophysics Supporting Research and Technology Grants Program, in order to focus a large fraction of the community's research efforts toward the goals of Astromag.

By conducting balloon flights at high geomagnetic latitudes (low geomagnetic cutoff) during solar minimum, some Astromag-type objectives are being realized, e.g. studies of antiprotons, positrons, and light-to-medium isotopes, albeit at energies substantially below those available with Astromag. The basis for several of the new investigations is the New Mexico State University (NMSU) balloon-borne magnetic spectrometer which was flown during the summer of 1987 in an effort to measure the flux and energy spectra of antiprotons over the interval between about 200 MeV and 1 GeV. The LEAP experiment also obtained very high precision data on the rigidity spectrum of protons and helium.

The next logical step following the LEAP experiment is a measurement of the positron flux. This experiment was conducted by a collaboration involving NMSU, the National Institute for Nuclear Physics, Frascatti, Italy (INFN), and the NASA Goddard Space Flight Center (GSFC), with Louisiana State University (LSU) participating through GSFC. The balloon flight apparatus, launched from Prince Albert, Canada, employed a new, tracking shower counter developed by the INFN group, as well as the time-of-flight (TOF) counter developed by the GSFC group for the LEAP instrument. The flight of this experiment (MASS) took place in summer, 1989. Our effort under this grant was devoted to analyzing the LEAP spectral data and to developing the hardware for the MASS experiment.

On-another-front, progress in the field of matter/anti-matter and isotope measurements in the cosmic rays depends upon improving the precision of the measurements of trajectories of particles through inhomogeneous magnetic fields. A possible solution here is the development of high resolution, solid state track detectors, that (i) can be employed in a strong magnetic field and (ii) can potentially be scaled up to the areas (~1 m^2) required for Astromag. A position resolution of 50 - 100 microns is currently possible, but this resolution (e.g. with multi-wire proportional counters and scintillating optical fibers) will be difficult to improve to

anything better than 25-30 microns; this accomplishment would itself be a formidable task! Therefore, totally new types of detectors should be pursued, and the development of solid state (silicon) detectors is one possibility. Strong interest in developing solid state track detectors followed the Astromag Study Team's identification of improved track detectors as one of the two highest priority technical needs for Astromag (the other is an efficient, innovative design for the magnet proper).

The realization of high quality position resolution over large areas for periods of more than a year will require detectors with excellent intrinsic spatial resolution and, of course, an adequate means to control/calibrate systematic effects that could degrade the measurements. For example, thermal control of the Astromag trajectory systems may be required to maintain dimensional stability, and accurate mapping of their responses will be needed for relating measured signals to absolute positions.

Thus, this project involved two areas of research and development, established as a collaborative venture between LSU and GSFC, with LSU personnel spending extended periods at GSFC. The first area, position sensitive detector development, utilized the detector development laboratories and facilities at GSFC, to investigate several types of detectors. The second area involved analysis of data from balloon experiments and has resulted in a Ph.D. being awarded to graduate student E. S. Seo.

A. Detector Development Studies

Several concepts for position sensitive detectors have been investigated including silicon drift chambers, scintillating optical fibers, silicon strip detectors and electron trapping materials. Results from each of these investigations are summarized below.

In a **Silicon Drift Chamber** (SDC) device, the drift time of the liberated charge is directly proportional to the point of impact of the charged particle. Such a device is shown schematically in Figure 1. The SDC is a 300 micron, 1 cm^2, fully depleted device. p^+ contacts on both surfaces provide a parabolic potential through which electrons are conducted by application of an additional voltage at a surface anode. Figure 2 shows an illustration of the potential configuration in the device.

To evaluate the position sensing ability of an SDC, a device was borrowed from Brookhaven National Laboratory. Beta particles were used to scan the surface of the detector using the arrangement shown in Figure 3. A histogram of arrival times was made for each position of the source. The source could be positioned repeatably to 20 microns while the collimator opening was 100 microns. We found that we could detect 50 micron shifts in the source position. Presumably, with a better collimator, this could have been improved. Figure 4 shows that the drift time across the device (the plot actually covers 2.5 mm of travel) was extremely linear, and gave a drift velocity of approximately 6 microns per nanosecond.

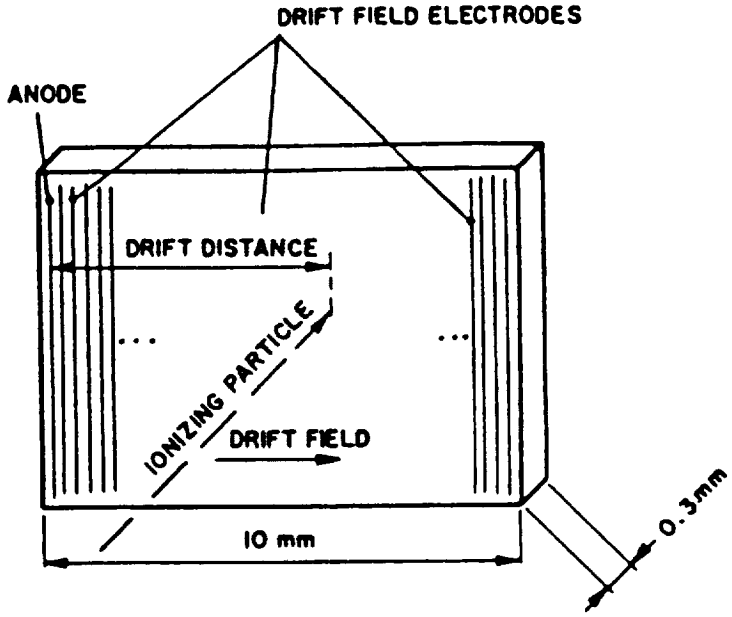

Figure 1. Schematic diagram of a typical silicon drift chamber. The wafer is about 0.3 mm thick and has a front area of a few cm^2. The surface is covered by a strip array of p^+n junctions which provides the depletion and the lateral drift field. (Only junctions at the extremes of the wafer are shown.) Electrons produced by the passage of a fast particle drift towards the anode, which is the only readout contact on the wafer.

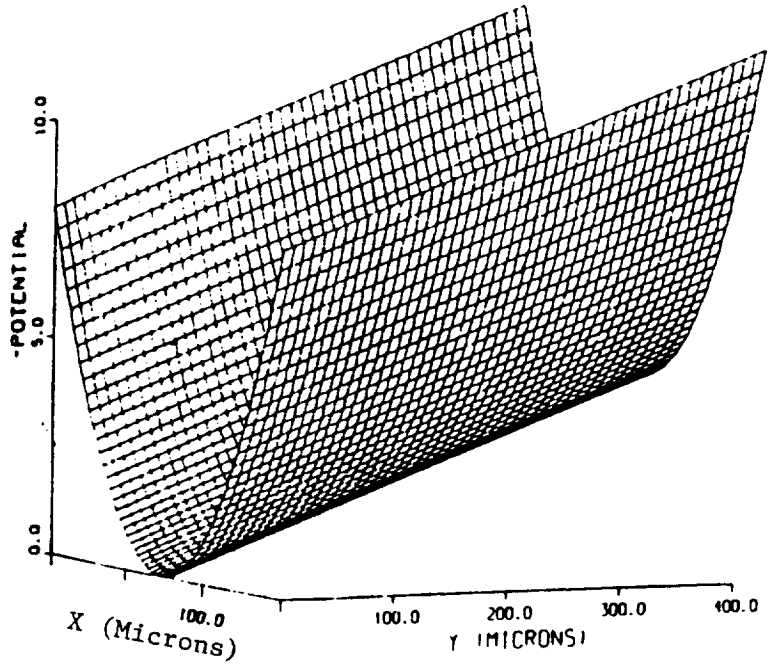

Figure 2: The negative potential of a fully depleted semiconductor detector when an additional linear lateral field along the y-axis is superposed. The field stabilizes the full depletion by sweeping away all generated charges.

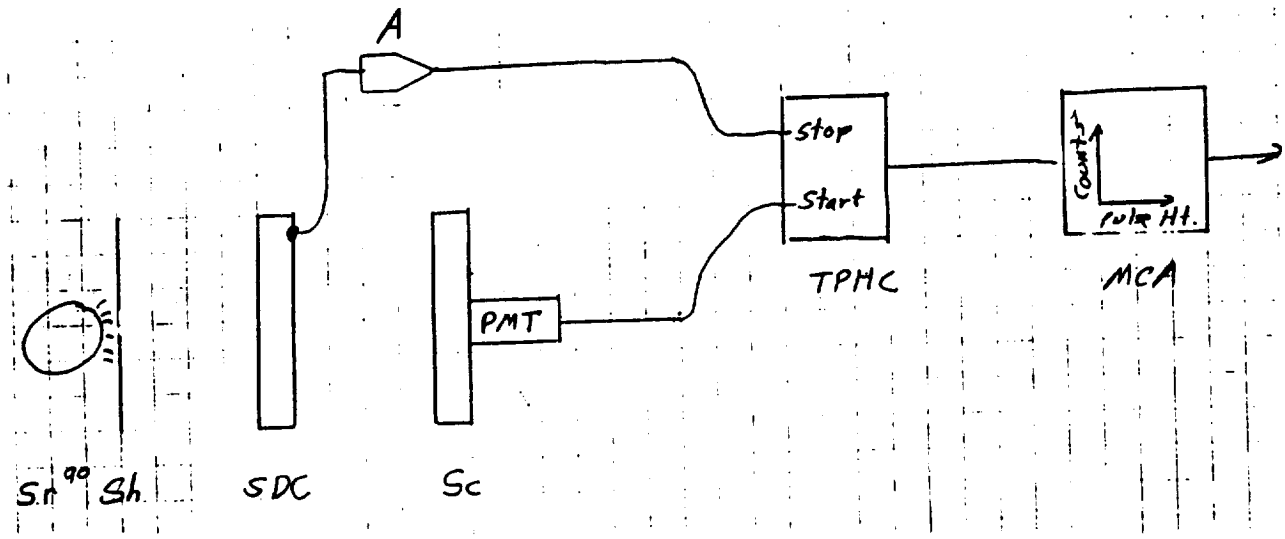

Figure 3: Schematic diagram of the testing configuration for the SDC. Radiation from a Sr^{90} β source, collimated by the Pb shield (Sh), passes through the Si drift chamber (SDC) and reaches scintillator (Sc) where it creates a light pulse that is detected by the photomultiplier tube (PMT). The signal from the anode of the SDC is amplified, shaped and delayed (A) before passing to the time-to-pulse-height convertor (TPHC) where it supplies the stop signal. The start signal comes from the PMT. Pulse heights (proportional to drift time) are analyzed in a multichannel analyzer (MCA), and the data is also sent to a computer for further analysis.

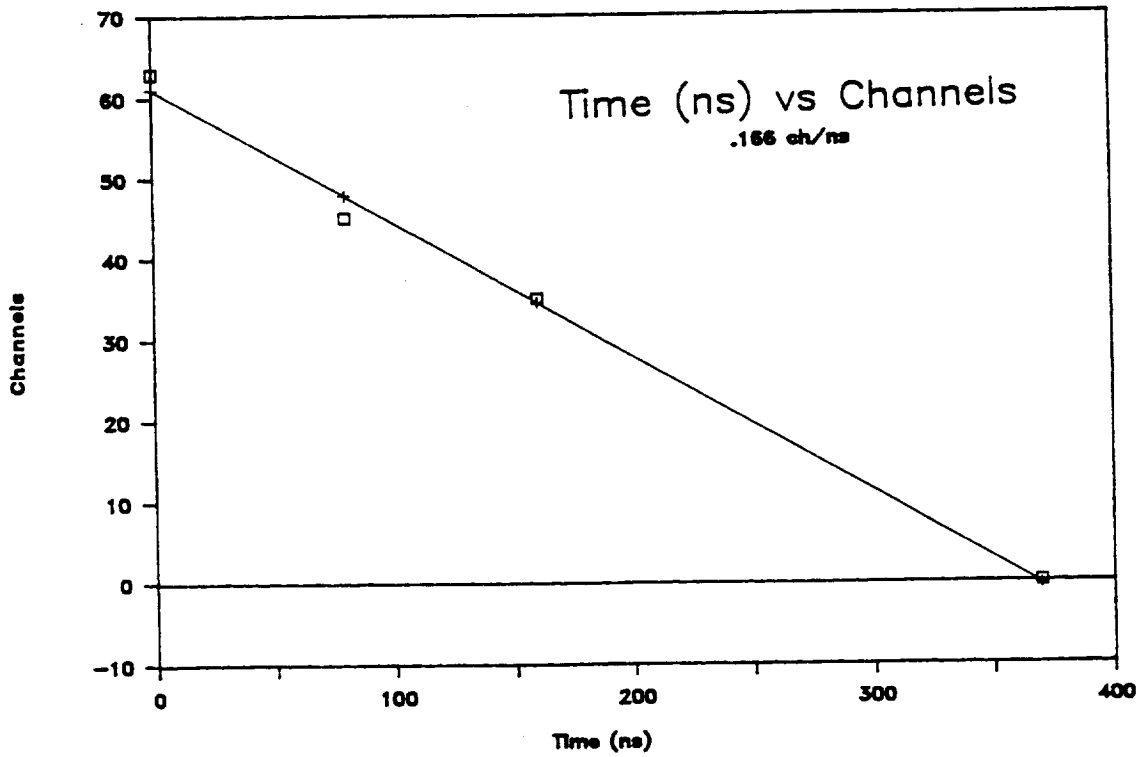

Figure 4: Results from a calibration of the SDC device.

Several attempts were made to fabricate SDC's in-house in the GSFC microelectronics lab. However this proved unsuccessful. The first batch of detectors all cracked during the processing. The devices made next all showed an unacceptably high noise level. This noise was caused by having exposed implanted regions on the surface and an improper annealing. A more critical problem, however, was the discovery that there is a strong temperature dependence to the electron drift time in this device. The high level of temperature control that would be necessary to maintain the position resolution would be extremely difficult in space, making the SDC's impractical in most applications. Other solid state position sensitive devices can provide equal resolution without this drawback.

A second effort was initiated, in conjunction with the Washington University (St. Louis) group, to study the use of **Scintillating Optical Fibers** in the space environment. WU produces these fibers (down to 100 microns in diameter) and has demonstrated that they can be used to measure heavy charged particles. The open question for a space experiment is "What is their stability in a changing thermal environment?" To answer this question, a series of measurements of the physical properties of the fibers (force to failure, tensile strength and Young's modulus) were undertaken, both for fiber strands and for fiber ribbons composed of many fibers mounted adjacent to one another on a substrate. Results of the mechanical tests are given in Tables 1 and 2.

Table 1

Table of Force to Failure, Tensile Strength, and Young's Modulus for Fiber Strand

Sample	Force to Failure (lbf)	Tensile Strength (psi)	Young's Modulus (psi) x 10^5
1	0.88	8,800	4.0
2	0.76	7,600	3.8
3	0.82	8,200	3.7
4	0.84	8,400	3.7
5	0.84	8.400	3.8
6	0.80	8,000	3.7
7	0.80	8,000	3.8
8	0.84	8,400	4.0
9	0.84	8,400	4.3
10	0.86	8,600	3.7
Average	0.83 ± .03	8,300 ± 300	3.9 ± 0.2

Table 2

Table of Force to Failure, Tensile Strength, and Young's Modulus for Fiber Ribbon

Sample	Force to Failure (lbf)	Tensile Strength (psi)	Young's Modulus (psi) x 10^5
1	9.6	8,000	6.1
2	9.0	7,500	5.8
3	14.2	11,800	5.6
4	14.6	12,200	5.6
5	14.6	12,200	5.6
6	10.0	8,300	5.7
7	9.4	7,800	5.6
8	10.8	9,000	5.2
9	13.0	10,800	5.0
10	12.0	10,000	4.6
11	14.4	12,000	5.8
12	14.2	11,800	5.4
13	13.6	11,300	5.2
14	13.0	10,800	5.1
15	13.6	11,300	5.2
Average	12.4 ± 2.1	10,300 ± 1,700	5.4 ± 0.4

Next, a mounting/testing apparatus for studying the change in the fibers as a function of temperature, was designed and constructed. The testing apparatus consisted of the following: (a) a rigid aluminum frame for mounting the fibers; (b) a thermally tight box in which we can control the temperature of the fiber array to +/- 1 degree. We then devised a method of testing the fibers by stimulating them with an ultraviolet lamp, focused down to a 50 micron spot size, through a fiber optic cable. The fiber array response was monitored for sensitivity and uniformity as a function of temperature by a CCD camera interfaced to a personal computer. Various temperature ranges typical of those encountered in space experiments were investigated. While thermal control will be necessary, the requirements on thermal design to maintain the stability and resolution of a fiber system are not stringent. Thus, fibers become an attractive position sensing option for certain types of experiments. (Such fibers have become a part of the LISA experiment which was selected for flight as one of the Astromag facility experiments.)

An alternate to SDC's is the **Silicon Strip Detector** (SSD). In these devices, shown schematically in Figure 5, conducting strips are implanted in the surfaces of a piece of n-type silicon. The charge liberated by the passage of a charged particle moves to the nearest one or two strips where it can be detected with suitable electronics. The detector fabrication technology has been developed extensively over the past several years, principally for use as vertex detectors in high energy accelerator experiments, and there are several companies that manufacture SSD's commercially. The advantage of an SSD is that the strip pattern can be adjusted to fit the experimental requirements. Strip spacings down to 5 microns have been successfully built and tested. In addition, strip patterns can be implanted on both surfaces of the device with the strips on one surface orthogonal to those on the other surface. This allows both an "X" and a "Y" coordinate to be determined from a single device. Further, the strip pattern may have a different spacing on the two surfaces, allowing the resolution to be "tuned" independently in each coordinate. This is indicated, for one particular design, in the lower part of Figure 5. In this application, the SSD's are to be used in a magnetic spectrometer. The particle "bend" dimension will be measured by the higher resolution top surface strips, while the orthogonal dimension requires a lower resolution.

The difficulties with SSD's for use in space application are environmental qualification and electronic readout. In the former case, we were able to test SSD's through thermal vacuum cycling and acoustic exposure to the degree necessary to verify that such devices can be space qualified. Additional work in this area is in progress.

The readout technique poses some complications, especially if there are a large number of strips in one or both dimensions. One potential scheme has been developed and tested at GSFC and involves "sparse readout." In this case, all strips are capacitively coupled and only every 4th or 5th strip is connected to a readout circuit, as illustrated in the center panel of Figure 5. Each circuit performs a pulse height analysis. The ratio of the signals is proportional to the charge division which then allows interpolation of the position at which the charged particle traversed the detector. This scheme is expected to give an average position resolution approaching 50 microns.

Another type of solid state detector with resolution comparable to the drift detectors is known as **Electron Trapping Material** (ETM). These materials have only very recently become available, and no detectors for cosmic rays have been built with them to date. ETM's operate much like thermoluminescence detectors which are widely used in dosimetry and dating applications. The ETM materials are wide gap semiconductors (Alkyline-earth sulfides) selectively doped to produce a quasiband and isolated trapping (metastable) states inside the intrinsic band gap as illustrated in Figure 6. Ionizing radiation excites electrons from the valence band of the material into the quasiband. About half of the excited electrons decay into trapping states, where they can remain for long periods of time. The remainder decay into the valence band, accompanied by prompt emission of light in the blue part of the spectrum. Note that no applied voltage is needed for these materials.

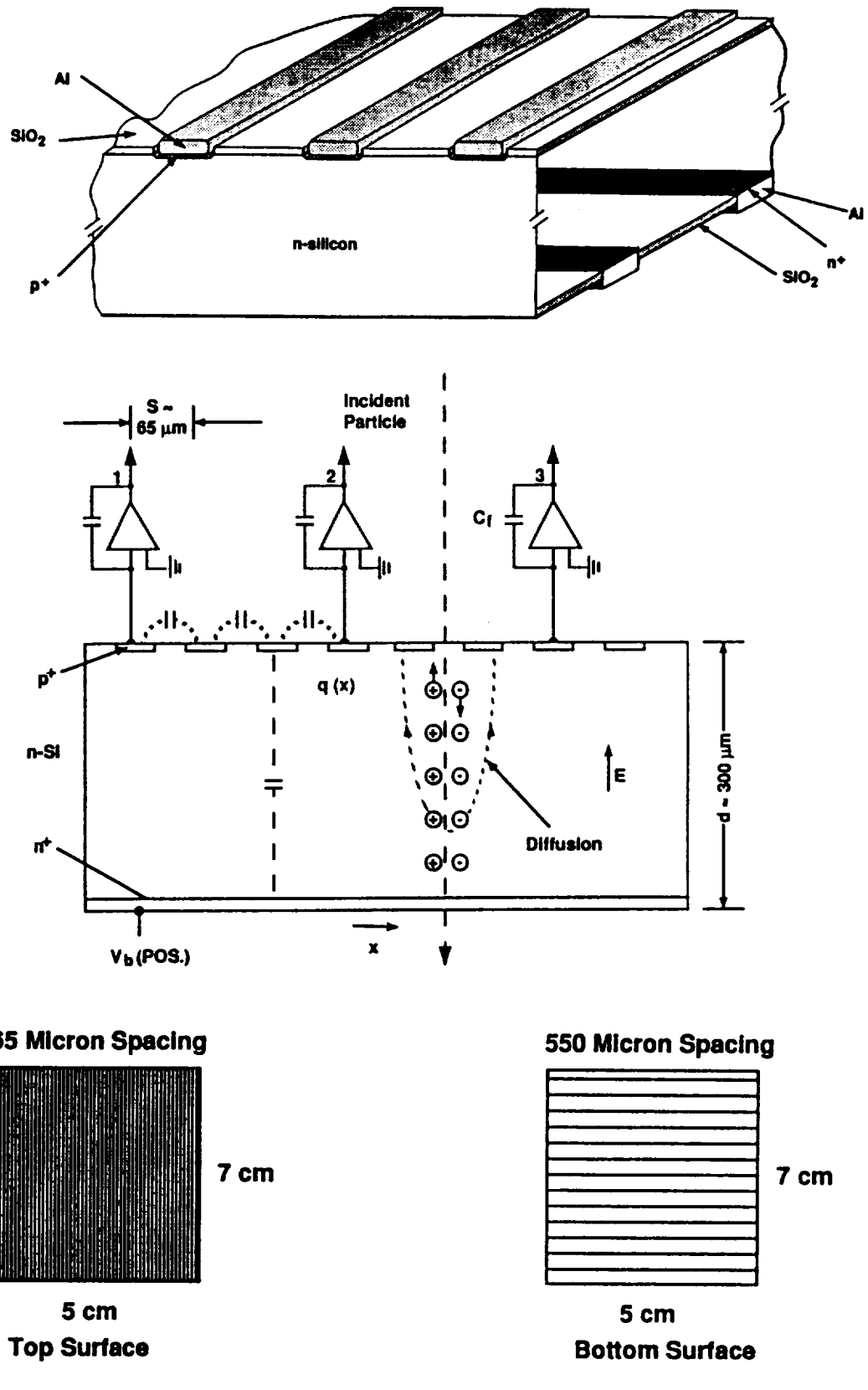

Figure 5: Schematic diagram of a silicon strip detector showing physical construction, operation and readout, and a "strawman" design having different strip spacing on the two surfaces.

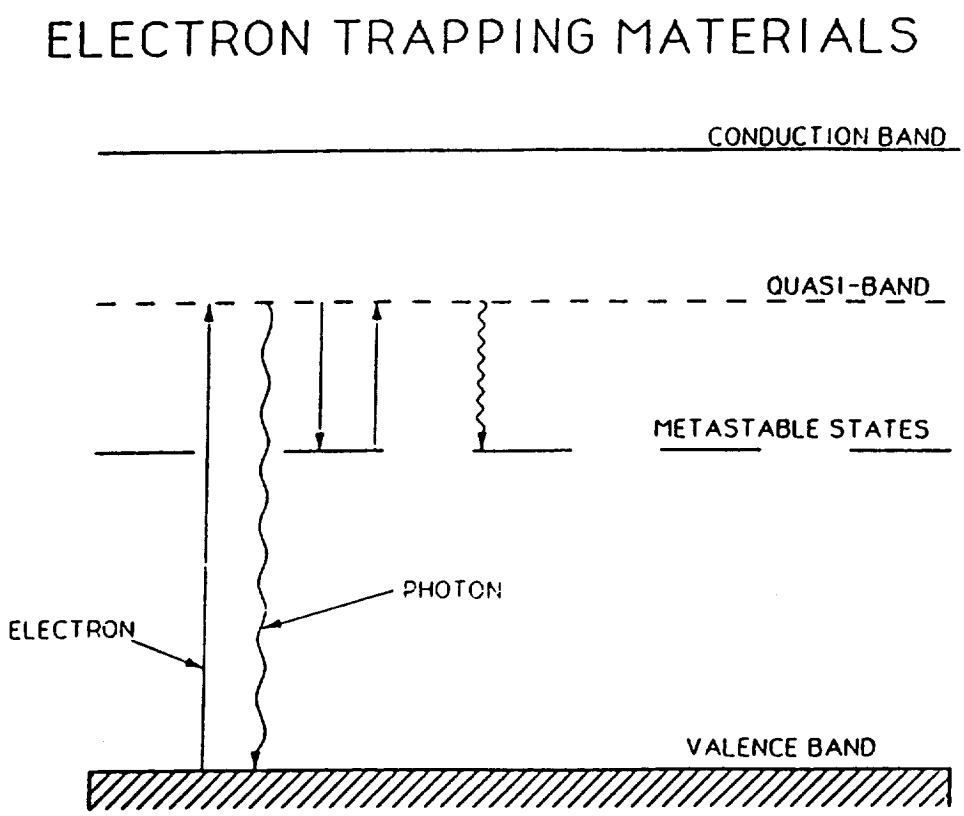

Figure 6: Operating Principle of an Electron Trapping Material. The quasi-band has energy E_c and the metastable states E_t.

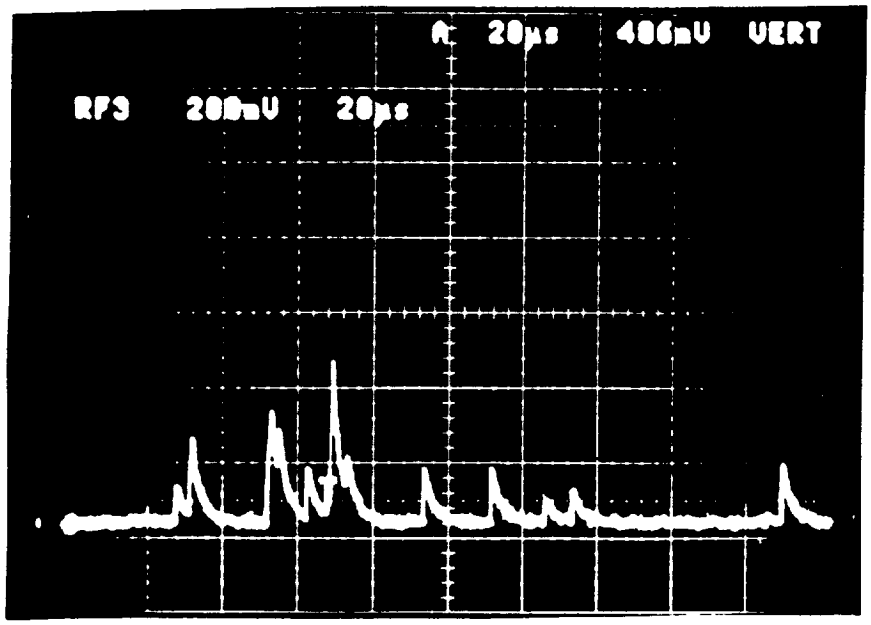

Figure 7: Oscilliscope traces showing pulse heights of stopping Alpha particles in a powdered sample of electron trapping semiconductor.

The electrons in the trapping levels are metastable and confined to a very small region around the trajectory of the incident particle. The location of the trapped electrons can be determined, to give the position at which the ionizing particle passed through the ETM, by forcing the electrons back into the quasi-band by application of stimulating infrared radiation. The electrons then return to the valence band emitting visible light from the spot at which the particle transited. This light pulse can be monitored by any number of detectors (PMT's, CCD's, etc.). Thus, the intrinsic position resolution is determined mainly by the thickness of the material. The practical resolution, however, depends upon the characteristics of the readout system.

The energy difference between the quasi-band and the valence band is typically ~2 eV. A relativistic proton will deposit ~600 eV/μm giving, for a 50 μm thick detector layer, about 15,000 excited electrons, of which ~7500 electrons remain trapped. Upon excitation, up to 7500 photons can be produced which, assuming a 20% light collection efficiency and a 15% photocathode efficiency, yields 225 photoelectrons. Thus, very thin detector layers are possible, especially for high-Z elements.

Laboratory tests have been carried out at GSFC on ETM detectors. A PMT is used to view the material which is stimulated by a laser beam to force the trapped electrons to leave the metastable state. Figure 7 shows an oscilloscope photograph of alpha particles at 5.4 MeV stopping in a sample. The peaks occur as the laser is swept across the sample, the scan rate and beam size can be used to infer the position resolution. To date, a high efficiency semiconductor material which is capable of resolving alpha particles at the 50 micron level has been produced.

The success of the early ETM studies has led to NASA awarding an SBIR grant to Quantex Corp. of Rockville, MD to investigate and produce "electron trapping semiconductors" for cosmic ray experiments. Material properties have been defined and evaluation tests for ETM samples have been developed. This effort is an on-going project between Quantex and GSFC.

A fast readout system for the ETM materials will be a necessity for their use in space experiments. Several schemes have been proposed and will be tested. For example, commercially available scanning systems can reach speeds of 40,000 steps/second and maintain 25 μm accuracy. At that rate, a read head could traverse 50 cm in 0.5 seconds. Light fed through a thick optical fiber on the head could uniformly irradiate 6-8 cm^2 which would be photographed by an image intensified CCD camera. To maintain sufficient readout speed it would be necessary to have an additional coarse position determining system, in order to tell the scanning head which 6-8 cm^2 block to interrogate. Alternatively, photon detectors could be placed around the periphery with a rotating ploygon directing the beam to scan across the surface. The drawbacks here are that very few photons would reach any particular photon detector, and the scan would introduce a long deadtime into the readout. The latter might be handled by recording events for 10-20 seconds, then stopping

and reading out all the spots in the ETM. Each event would then be reconstructed off-line. For this to work a coarse positioning system would still be required. Discriminating against charged particle background might also present a problem.

Despite the potential problems that an ETM system presents, it offers a very real possibility of achieving significant improvements in position resolution and deserves careful evaluation and testing. The readout speed may limit the size of the ETM planes that can be utilized, and configurations involving mosaics of many individual detector planes may be indicated. Clearly, much additional development work remains to be done.

B. Particle Astrophysics Investigations from Balloons

The effort in this area has focused on the NASA NMSU Balloon Borne Magnet Facility shown schematically in Figure 8 in its 1987 and 1989 configurations. Note that the major difference is the inclusion of the gas Cherenkov counter and an imaging calorimeter in 1989 replacing a solid Cherenkov counter (C) in the 1987 configuration. This emphasizes the versatility of the BBMF. It can be reconfigured with a variety of ancillary detectors to perform different scientific investigations. Under this grant, graduate student E. S. Seo worked with the installation and calibration of the Time-of-Flight System (T1, T2, T3, T4) plus flight operations for the 1989 experiment, but analyzed the experimental data from the 1987 flight of BBMF. The following summary focuses upon the data analysis and astrophysical interpretation.

The three major components provided by the BBMF for the 1987 LEAP flight were the magnet, the multiwire proportional counter (MWPC) tracking system and the electronics readout/telemetry system. The 150 kg superconducting magnet is an 80 henry inductor wound with copper-clad, 54 filament NbTi wire. The current in the coil (inside diameter 36 cm, outside diameter 61 cm, and axial thickness 10 cm) is 1.39×10^6 Amp-turns and produces a magnetic field of 40 kG at the center of the coil (operating current of 120 amperes).

The multiwire proportional counters (MWPC's) used for trajectory measurements provide spatial resolution of ~125 μm in one direction and 500 μm in the other direction. They are oriented so that the high resolution coordinate is perpendicular to the axis of the magnet. Eight high-resolution and four low-resolution measurements are made for each charged particle track.

The Time-of-Flight system employs Pilot B scintillator pickets viewed at both ends by 2" RCA 8575 PMTs. A picket consists of two paddles, each viewed by one PMT. The top planes (T1, T2) consist of 6 pickets. The bottom planes (T3, T4) consist of 4 pickets separated from the top plane by 1.9 m. The Cherenkov detector (C) is the final counter traversed by each particle. The fluorocarbon liquid FC-72 with a refractive index of 1.255 provides essentially 100% rejection of μ^-, π^-, and K^-.

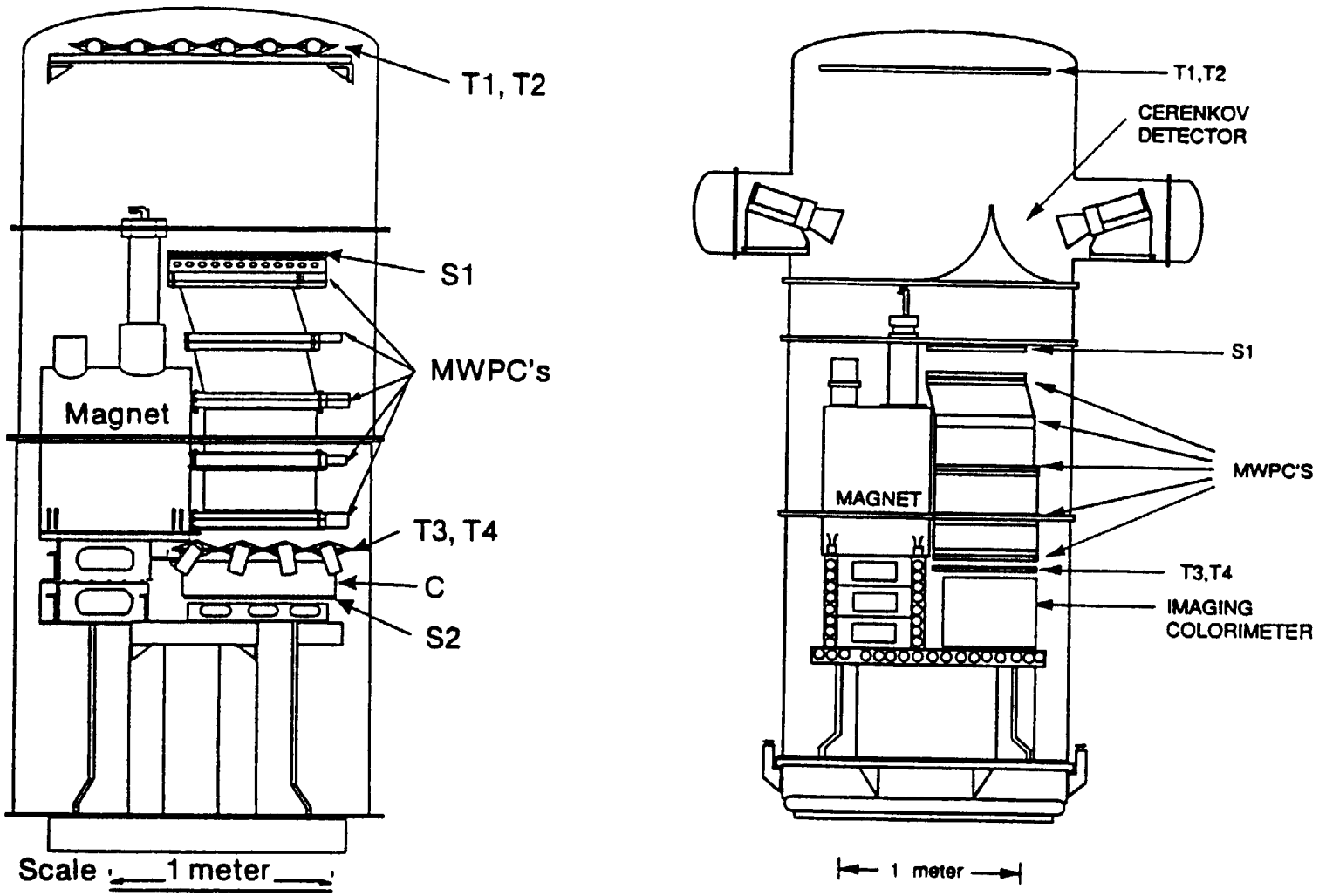

Figure 8: The NASA NMSU Balloon Borne Magnet Facility (BBMF) configured for the 1987 LEAP (left) and 1989 MASS (right) flights.

The 70 cm x 70 cm x 10 cm active volume is viewed by six 5-inch "teacup" PMTs, with each PMT output pulse height recorded separately.

Particle charge is measured by the scintillator (S1) and rigidity by the magnet. The TOF and Cherenkov provide additional velocity information, and the TOF identifies upward moving, "splash albedo" particles. By combining the measurements from the different subsystems, it was possible to:

1) Obtain accurate rigidity spectra for Hydrogen and Helium,
2) Examine Geomagnetic Cut-off's for the balloon flight
3) Measure the spectra of atmospheric secondaries and splash albedo, and
4) Investigate the p/He ratio as a function of energy, focussing upon reacceleration effects.

Details of the analysis techniques and methods can be found in the attachments or in Seo's Ph.D. dissertation and will not be described here. Only the scientific results will be summarized.

1. Geomagnetic Cut-off and Splash Albedo:

The theory of charged particle motion in the geomagnetic field predicts that cosmic rays with a magnetic rigidity below a certain value will be deflected enough to miss the earth entirely for a given incident direction. The smallest momentum at which all directions are allowed, R_c, the geomagnetic cutoff, increases rapidly as latitude decreases. The effects of the varying geomagnetic cutoff were observed in the proton data collected along the balloon trajectory, Figure 9, which also shows lines of constant, nominal, calculated cutoff rigidity from 0.6 - 1.1 GV. Proton spectra from the "start" and "end" of the flight are compared in Figure 10. The instrumental range cutoff is at ~0.45 GV. The observed spectrum results from the superposition of two spectra: the primary proton spectrum, with geomagnetic cutoff effects, and the atmospheric secondary spectrum, which decreases with increasing rigidity. The difference between the spectra observed near the start and the end of the flight reflects the varying geomagnetic cutoff.

The primary proton spectrum was obtained by subtracting a calculated secondary proton spectrum at 5 g/cm^2 from the measured spectrum at the top of the LEAP instrument. The normalization for the secondary proton spectrum was obtained by matching the initial and final spectra at high (>few GV) rigidity. Figure 11 shows the primary proton spectra at the top of the atmosphere for the three selected intervals along the balloon trajectory. The "measured" geomagnetic cutoffs in these intervals were taken to be the values where the primary protons were 50% of their values in the absence of any cutoffs, and these are compared in Table 3 to the nominal cutoffs expected from detailed orbit calculations based on the Earth's surface field. The measured values are ~25% below the calculated cutoffs.

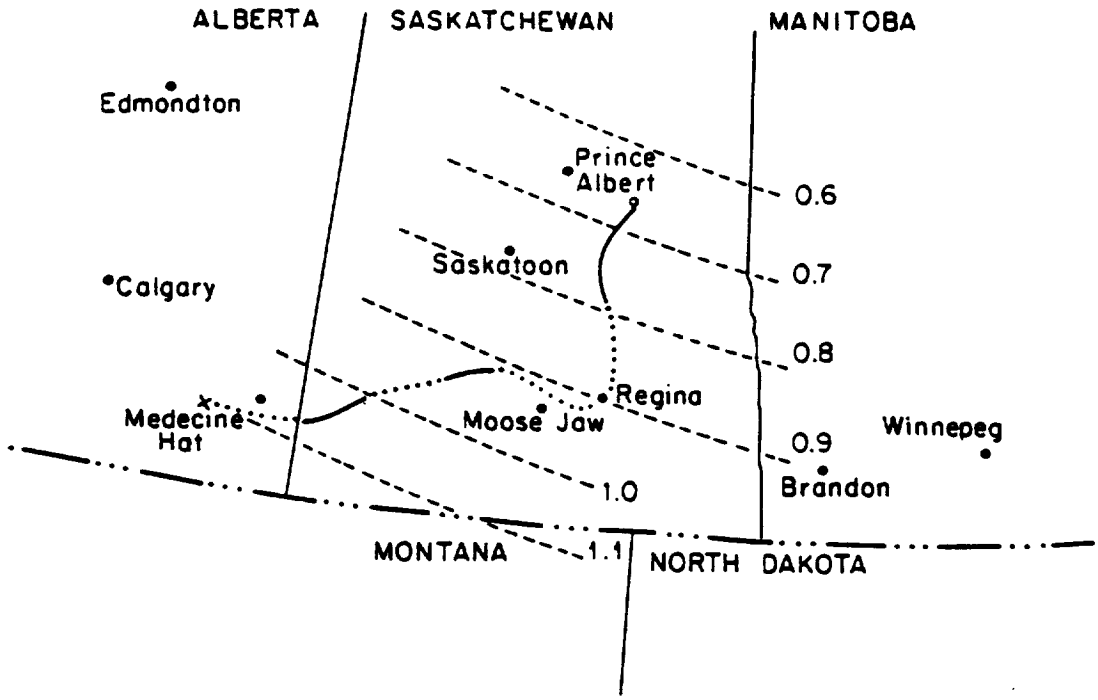

Figure 9: Trajectory of the LEAP flight from launch near Prince Albert to termination near Medecine Hat. The solid portions indicate three time periods (start, middle and end) selected for cutoff analysis.

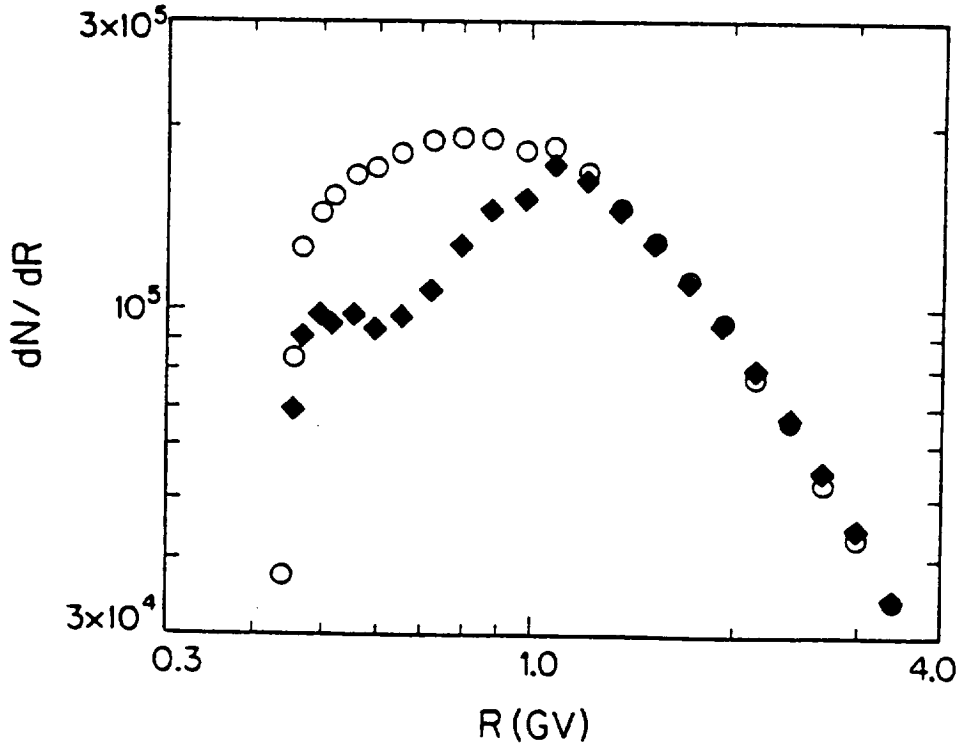

Figure 10: Proton spectra from the start (circles) and end (diamonds) portions of the flight.

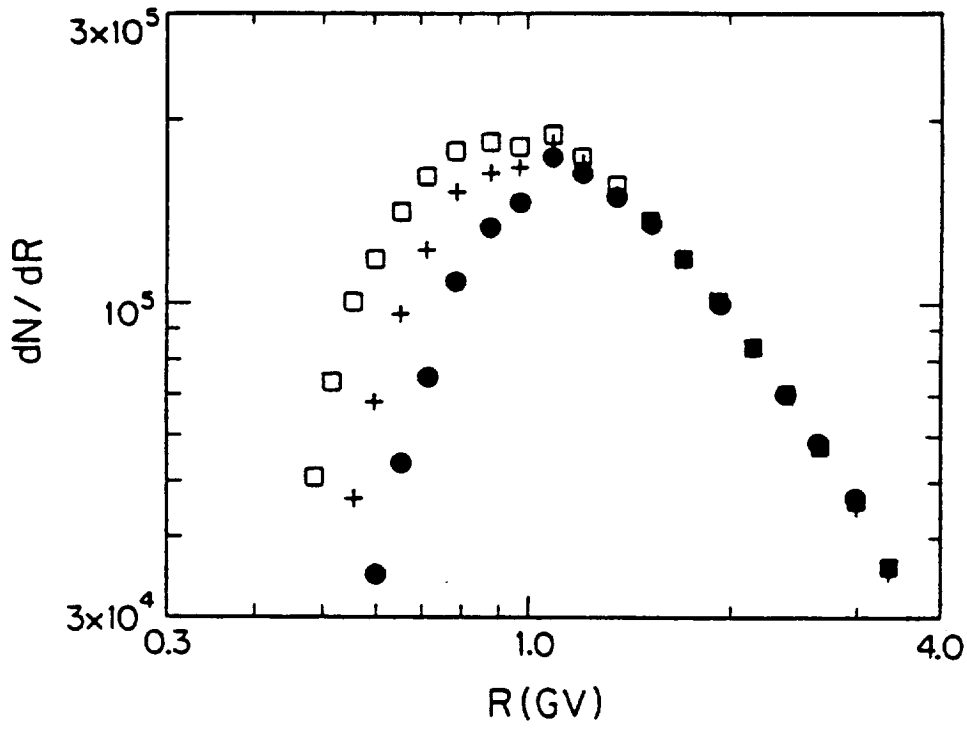

Figure 11: Primary protons at the top of the atmosphere for the "start" (❑), "middle" (+), and "end" (●) of the flight.

Table 3

Comparison of nominal and measured cutoffs along the LEAP trajectory.

	Start	Middle	End
Interval Start	255.7 E, 52.7 N	253.3 E, 50.7 N	251.0 E, 50.3 N
Interval Stop	255.5 E, 51.5 N	252.5 E, 50.7 N	250.2 E, 49.9 N
Nominal R_c (GV)	0.66 - 0.78	0.92 - 0.94	1.02 - 1.09
Measured R_c (GV)	0.54	0.68	0.79

The timing data from the TOF counters permitted determination of the splash albedo, which often constitutes an unwanted background for balloon experiments. Splash albedo protons were selected with the same criteria as other protons, except for their negative track deflection and negative velocity (upward moving) direction. Figure 12 shows the observed splash albedo spectra for singly-charged particles, including protons, kaons, pions, muons, and electrons. Using the TOF to identify protons, it was found that the bump just below 1 GV in the Z = +1 albedo spectrum is due to the proton component. Table 4 summarizes the observed ratios of albedo protons to downward moving protons as a function of rigidity. This ratio decreases with rigidity as approximately R^{-4}.

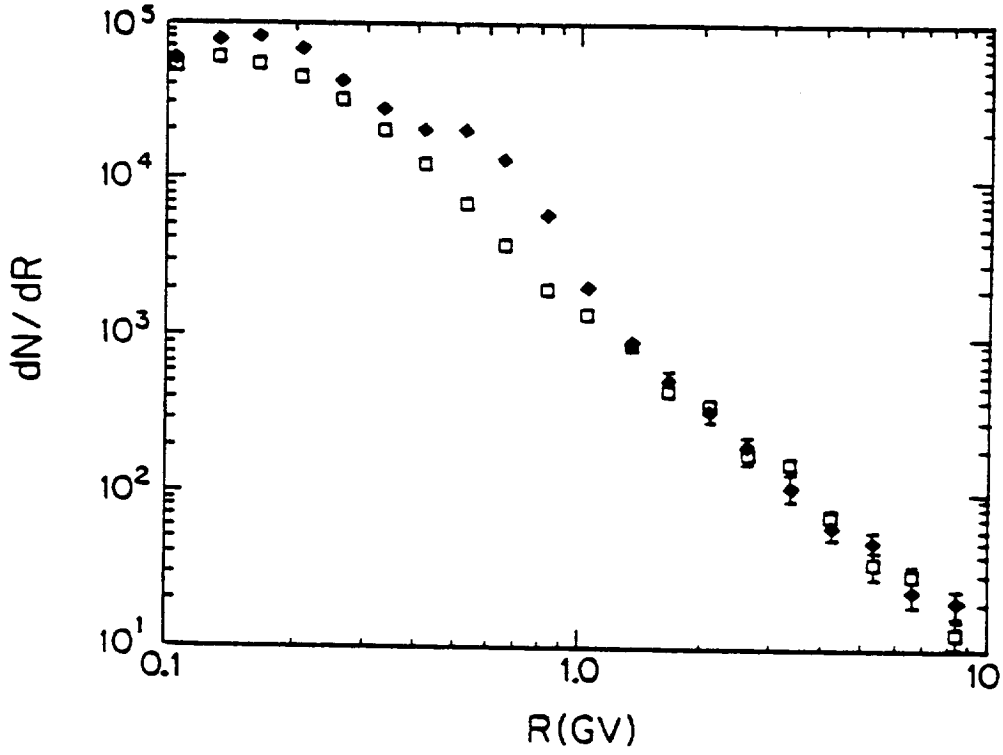

Figure 12: Splash albedo spectra for Z = +1 (◆) and Z = -1 (❑) particles .

Table 4

Observed ratio of Albedo to downward moving protons.

R (GV)	Ratio
0.562 - 0.631	$(2.34 \pm 0.13)10^{-2}$
0.631 - 0.708	$(1.54 \pm 0.09)10^{-2}$
0.708 - 0.794	$(1.15 \pm 0.07)10^{-2}$
0.794 - 0.891	$(6.0 \pm 0.5)10^{-3}$
0.891 - 1.0	$(3.5 \pm 0.4)10^{-3}$

2. Particle Energy Spectra

The differential energy spectrum involves the instrument geometric factor (330 cm^2sr for LEAP), the flight time, corrected for the dead time (~30%) and the particle detection efficiency. The latter was determined from the fraction of particles that passed the selection criteria, principally positive TOF and a reconstructable trajectory. The overall efficiency was ~33%. The resulting spectra, corrected to the top of the atmosphere, are shown in Figure 13 along with IMP-8 satellite data from nearly the same time period as the LEAP flight. The overall flux uncertainty is 10-15%, due mainly to uncertainty in the overall instrument efficiency, and this may move the spectrum up or down, but would not affect the spectral shape.

Above 10 GV the spectra follow a rigidity power law with spectral indices of 2.74 ± 0.02 for protons and 2.68 ± 0.03 for helium. These results agree with the index 2.70 ± 0.05 for both species measured with the same magnet spectrometer in 1976 and 1979. While numerous experiments have been performed to study protons and helium, few direct measurements significantly greater than 10 GV have been made, and none has covered the LEAP energy range (0.5 - 100 GV) with a single instrument.

A spherically symmetric model of solar modulation, in which cosmic rays propagating through the solar wind are subjected to (1) diffusion through the turbulent magnetic fields, (2) convection by the outward motion of the field imbedded in the solar wind, and (3) adiabatic deceleration by the expansion of the fields as they propagate away from the sun, has been employed. Assuming that the local interstellar spectra of protons and helium at the heliospheric boundary are described by the LEAP high energy spectra, $\sim AR^{-2.74}$ and $\sim BR^{-2.68}$, respectively, for protons and helium, modulation to the orbit of earth has been performed to obtain the best fit to the 1987 LEAP measurements. The normalization constants A and B were chosen to match the LEAP data near 100 GeV/nucleon, where the modulation effect is negligible. The sets of modulated spectra, representing various modulation parameters, are shown with the LEAP and IMP-8 data in Figure 14 for, from top,

a) No modulation, $\phi = 0$,
b) $\phi = 200$ MV, (c) $\phi = 400$ MV,
d) $\phi = 500$ MV (e) $\phi = 600$ MV
f) $\phi = 800$ MV (g) $\phi = 1000$ MV,

where the energy loss due to solar modulation is $\Delta E = ze\phi$ and ϕ is the modulation parameter.

The LEAP data are well fit by a value of $\phi = 500$ MV. The solar modulation parameter for solar minimum has previously been estimated to be 300 - 600 MV by fitting the measured electron spectrum using the local interstellar electron spectrum

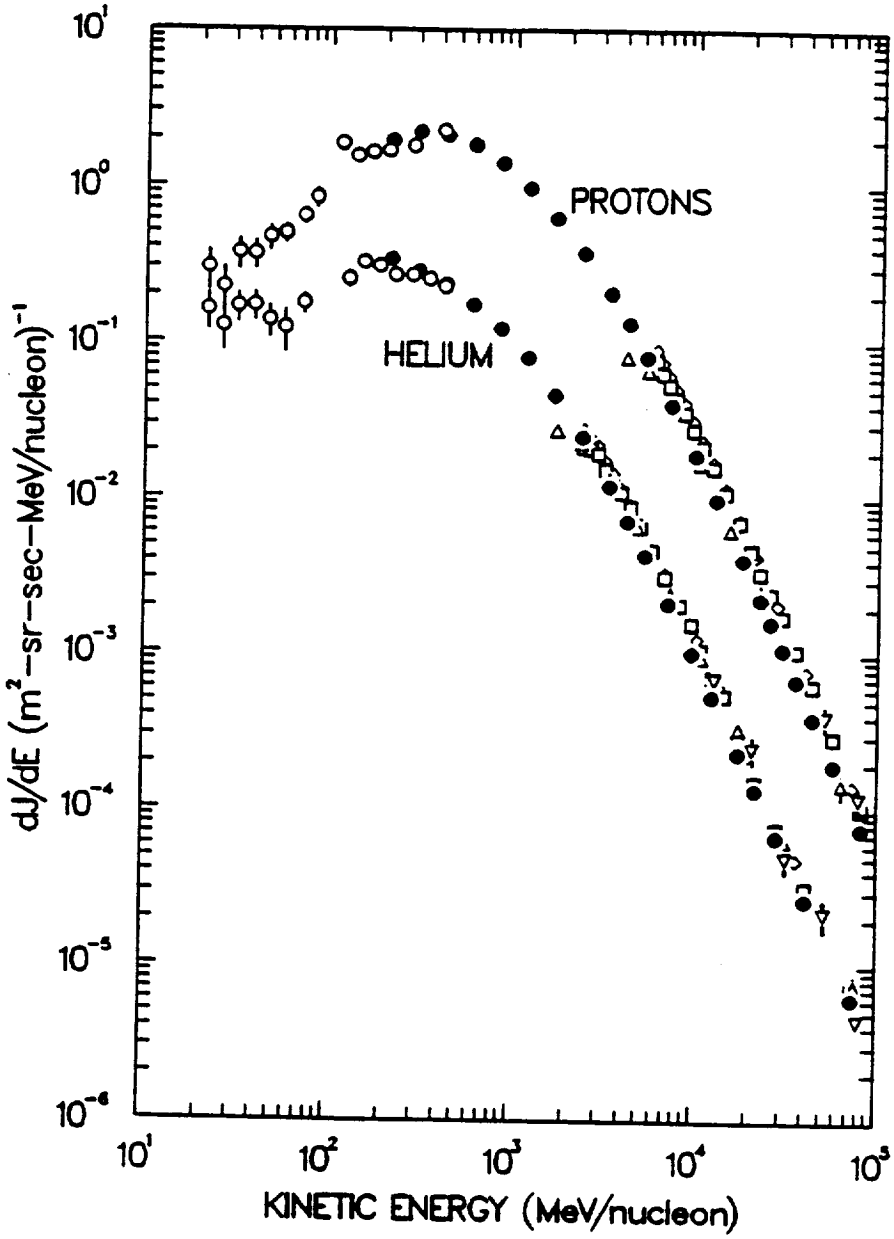

Figure 13: Differential energy spectra for cosmic ray protons and helium nuclei measured in 1987 (● for LEAP; O for IMP-8, from Reames, 1990) along with previous balloon measurements: ◇ (76 data, □ (79 data), Webber et al. (1987); ▽, Ryan et al. (1972); △, Smith et al. (1973).

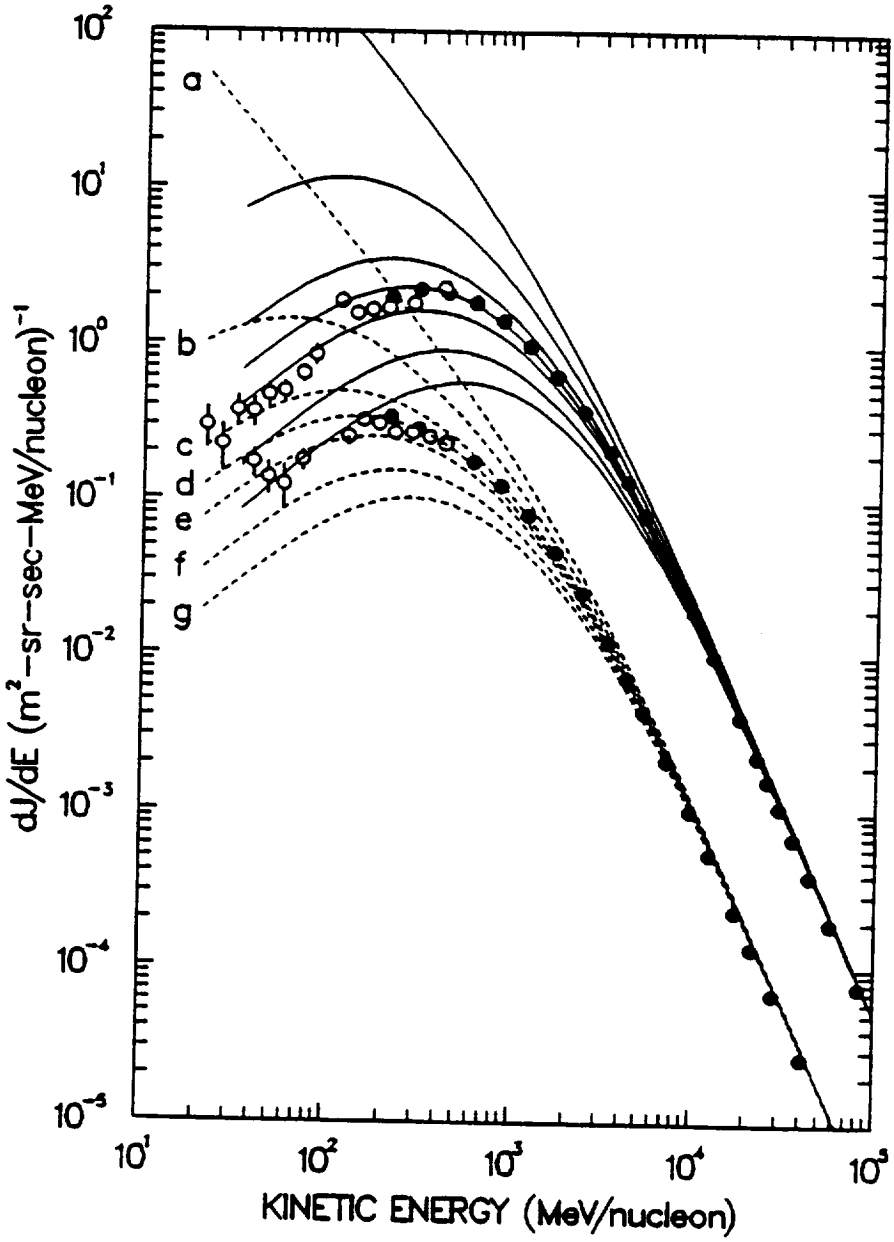

Figure 14. Differential energy spectra for cosmic ray protons and helium nuclei in 1987 (closed circles for LEAP, open circles for IMP-8). The two sets of curves represent the local interstellar and modulated spectra for protons (solid lines) and helium (dashed lines).

deduced from the galactic non-thermal radio emission. It has also been estimated to be 450 ± 100 MV from the quartet of primary and secondary isotopes ^{1}H, ^{2}H, ^{3}He, and ^{4}He. These estimates are in good agreement with our value of 500 MV. Therefore, rigidity power law spectra appear to be reasonable forms for the proton and helium interstellar spectra above 200 MeV/nucleon.

3. Reacceleration Effects

Since higher energy cosmic rays escape more readily from the Galaxy, any spectral modifications introduced by re-acceleration during propagation in the interstellar medium would be energy dependent. This effect should be especially noticeable for light elements, particularly protons and helium, whose interaction mean free paths are much longer than their escape mean free paths. The effects of re-acceleration have been examined by comparing the LEAP observations with published calculations of the p/He ratio done with a distributed re-acceleration model.

The p/He ratios from the LEAP experiment are shown in Figure 15 along with previous measurements and compared with the calculated curves for the p/He ratios near the earth at solar minimum including re-acceleration. The calculated curves are normalized to the high energy (~100 GeV/nucleon) LEAP data in the top panel and to the low energy (~1 GeV/nucleon) LEAP data in the bottom plot. In both parts of Figure 15 the solid curves are based on rigidity-dependent propagation with power law injection spectra in rigidity, while the dashed curves are for momentum-dependent propagation with power law spectra in momentum. When the curves are normalized to fit the high energy data, the calculated ratios are 10-30% higher than the low energy results, whereas when the curves are normalized to fit the lower energy data the calculated ratios fall ~30% below the high energy data. In the latter case, an extrapolation of the curves to higher energies agrees with the JACEE ratio of 12 ± 3.6 above 2 TeV/nucleon, but neither normalization is able to fit the full range of the LEAP measurements.

Figure 16 compares the measurements with calculated p/He ratios without re-acceleration. The symbols and curves are the same as in Figure 15. When the curves are normalized to fit the high energy data (Figure 16, top), the calculated ratios corresponding to rigidity spectra with rigidity dependent propagation (solid curve) agree well with the LEAP data. However, the dashed curves corresponding to momentum spectra with momentum dependent propagation are about 30% lower than the measured ratios. On the other hand, when the momentum dependent dashed curve is normalized to fit the low energy LEAP data, as shown in the bottom panel, the calculated ratios are about 50% higher than the high energy LEAP data.

In summary, the comparisons in Figures 15 and 16 show that the data do not support re-acceleration but do agree with the case of no re-acceleration during propagation that is dependent on rigidity with an injection spectrum that is a power law rigidity. Even though there is an uncertainty of 10-15% in the absolute value of the p and He spectra, the shape of the p/He ratio should remain unaffected. It is this energy dependence that does not support re-acceleration at the level included in the theoretical calculations. This is the first, new, significant, experimental test of the re-acceleration theories that has become available!

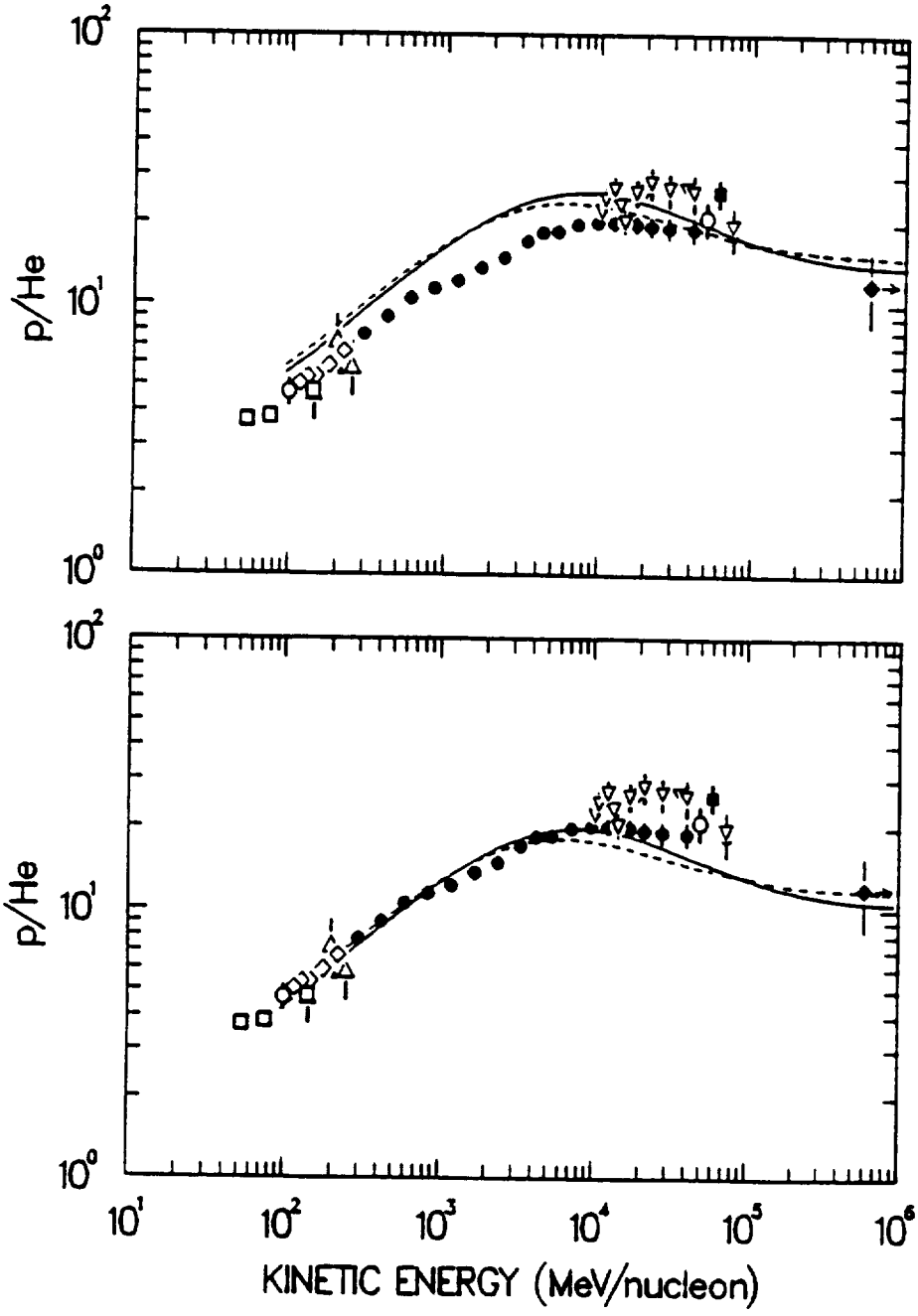

Figure 15. Proton to helium ratio data as a function of energy compared with calculations of the p/He ratios near the earth with re-acceleration.

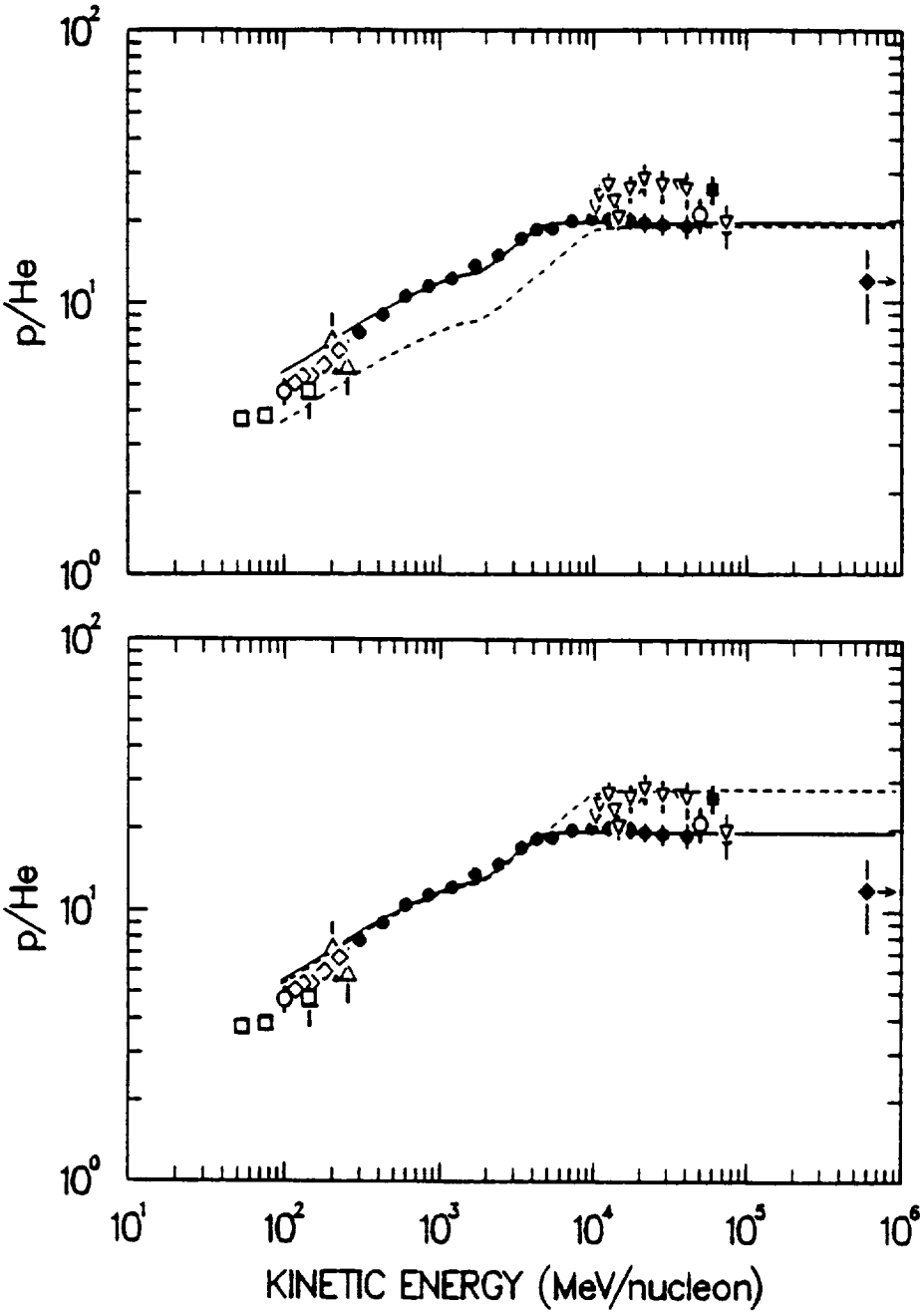

Figure 16. Proton to helium ratio data as a function of energy compared with calculations of the p/He ratios near the earth without re-acceleration.